CHIN. PHYS. LETT. Vol. 38, No. 2 (2021) 024201

Moderate-Temperature Near-Field Thermophotovoltaic Systems with Thin-Film InSb Cells

Rongqian Wang(王荣倩)[1*], Jincheng Lu(陆金成)[1,2], and Jian-Hua Jiang(蒋建华)[1*]

[1]*School of Physical Science and Technology & Collaborative Innovation Center of Suzhou Nano Science and Technology, Soochow University, Suzhou 215006, China*

[2]*Center for Phononics and Thermal Energy Science, China-EU Joint Center for Nanophononics, Shanghai Key Laboratory of Special Artificial Microstructure Materials and Technology, School of Physics Science and Engineering, Tongji University, Shanghai 200092, China*

(Received 12 October 2020; accepted 21 December 2020; published online 27 January 2021)

Near-field thermophotovoltaic systems functioning at 400–900 K based on graphene-hexagonal-boron-nitride heterostructures and thin-film InSb p–n junctions are investigated theoretically. The performances of two near-field systems with different emitters are examined carefully. One near-field system consists of a graphene-hexagonal-boron-nitride-graphene sandwiched structure as the emitter, while the other system has an emitter made of the double graphene-hexagonal-boron-nitride heterostructure. It is shown that both systems exhibit higher output power density and energy efficiency than the near-field system based on mono graphene-hexagonal-boron-nitride heterostructure. The optimal output power density of the former device can reach 1.3×10^5 W/m^2, while the optimal energy efficiency can be as large as 42% of the Carnot efficiency. We analyze the underlying physical mechanisms that lead to the excellent performances of the proposed near-field thermophotovoltaic systems. Our results are valuable toward high-performance moderate temperature thermophotovoltaic systems as appealing thermal-to-electric energy conversion (waste heat harvesting) devices.

DOI: 10.1088/0256-307X/38/2/024201

Thermophotovoltaic (TPV) systems are solid-state renewable energy resource that is of immense potentials in a wide range of applications including solar energy harvesting and waste heat recovery.[1−10] In a TPV system, a photovoltaic (PV) cell is placed in the proximity of a thermal emitter and converts the thermal radiation from the emitter into electricity via infrared photoelectric conversion. However, the frequency mismatch between a moderate-temperature thermal emitter and the PV cell leads to significantly reduced performance of TPV systems at moderate temperatures (i.e., 400–900 K, which is the majority spectrum of the industry waste heat). To overcome this obstacle, materials which support surface polaritons have been used to introduce a resonant near-field energy exchange between the emitter and the absorber.[6,9,11−14] As a consequence, near-field TPV (NTPV) systems have been proposed to achieve appealing energy efficiency and output power.[12,15−22] Near-field systems based on graphene, hexagonal-boron-nitride (h-BN) and their heterostructures have been shown to demonstrate excellent near-field couplings due to surface plasmon polaritons (SPPs), surface phonon polaritons (SPhPs) and their hybridizations [i.e., surface plasmon-phonon polaritons (SPPPs)].[11,13,23−27] It was demonstrated that a heterostructure consisting of graphene–h-BN multilayers performs better than the monocell structure, and the heat flux is found to be three times larger than that of the monocell structure.[25−27] Here, we consider a graphene–h-BN–graphene sandwiched structure and a graphene–h-BN–graphene–h-BN four-layer structure as the near-field thermal emitters to provide the enhanced radiative heat transfer.

In order to convert the infrared radiation into electricity, the energy bandgap ($E_{\rm gap}$) of the NTPV cell (i.e., the p–n junction) must match the radiative spectrum generated by the emitter. Ⅲ–Ⅴ group compound semiconductors like gallium arsenide (GaAs), gallium antimonide (GaSb), indium antimonide (InSb) and indium arsenide (InAs) have been used because of their small bandgap energy, high electron mobility and low electron effective mass.[9,12,16,23] Recently, semiconductor thin-films have been explored in NTPV systems. In Refs. [9,22], an NTPV system based on an InAs thin-film cell exhibits appealing performance operating at high temperatures. However, the system suffers from low energy efficiency (below 10%) when operating at moderate temperature due to the parasitic heat transfer induced by the phonon-polaritons of InAs. Here, we take InSb as the near-field absorber since the bandgap energy of InSb is lower compared

Supported by the National Natural Science Foundation of China (Grant Nos. 11675116 and 12074281), the Jiangsu Distinguished Professor Funding, a Project Funded by the Priority Academic Program Development of Jiangsu Higher Education Institutions (PAPD), and the China Postdoctoral Science Foundation (Grant No. 2020M681376).

*Corresponding authors. Email: rongqianwang@sina.com; jianhuajiang@suda.edu.cn

© 2021 Chinese Physical Society and IOP Publishing Ltd

to InAs and its photon-phonon interaction is much weaker than InAs. For the temperature of the InSb cell, $T_{\rm cell} = 320\,{\rm K}$, which has been proved to be an optimal cell temperature in our previous work,[28] the gap energy is $E_{\rm gap} = 0.17\,{\rm eV}$ and the corresponding angular frequency is $\omega_{\rm gap} = 2.5 \times 10^{14}\,{\rm rad/s}$.

In this work, we examine the performances of two NTPV devices: the graphene–h-BN–graphene–InSb cell (denoted as G-FBN-G-InSb cell, with the graphene–h-BN–graphene sandwiched structure being the emitter and the InSb thin-film being the cell) and the graphene–h-BN–graphene–h-BN–InSb cell (denoted as G-FBN-G-FBN-InSb cell, with the double graphene–h-BN heterostructure being the emitter and the InSb thin-film being the cell). We study and compare the performances of these two systems and reveal their underlying physical mechanisms. We further optimize the performance of the near-field TPV systems for various parameters.

In this work, first we try to optimize the design of the h-BN–graphene heterostructures as the emitter to improve the performance of the NTPV system. Then, we try to discuss the effect of finite thickness of the InSb cell on the performance of the NTPV system. In the following, firstly we describe our NTPV system and clarify the radiative heat flux exchanged between the emitter and the cell. Secondly, we study and compare the performances of the two NTPV systems, and analyze the spectral distributions of the photo-induced current density and incident heat flux. We also study the photon tunneling coefficient to further elucidate the physical mechanisms. Thirdly, we examine the performances of the two NTPV systems for various InSb thin-film thicknesses and emitter temperatures to optimize the performances of the NTPV systems. Finally, we give conclusions.

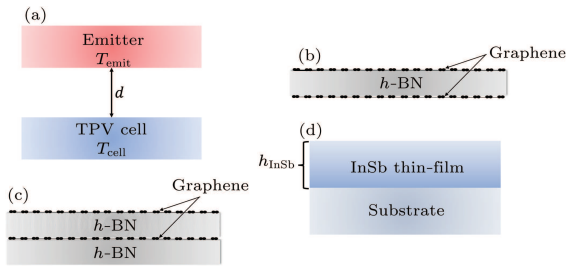

Fig. 1. Schematic illustration of the NTPV systems. (a) A representative TPV device. A thermal emitter of temperature $T_{\rm emit}$ is located at a distance d of a thermophotovoltaic cell of temperature $T_{\rm cell}$. Two compositions of the thermal emitter with (b) the graphene–h-BN–graphene structure and (c) the graphene–h-BN–graphene–h-BN structure. (d) The thermophotovoltaic cell with an InSb thin film with thickness $h_{\rm InSb}$ supported by a semi-infinite substrate.

System and Theory. In Fig. 1, we consider the graphene–h-BN–InSb NTPV systems. Figure 1(a) is a schematic presentation of a typical NTPV system, which consists of a thermal emitter and a thermophotovoltaic cell. The emitter and the thermophotovoltaic cell is separated by a vacuum gap with thickness d. The temperatures of the emitter and cell are kept at $T_{\rm emit}$ and $T_{\rm cell}$, respectively. The thermal radiation from the emitter is absorbed by the cell and then converted into electricity via photoelectric conversion. Figures 1(b) and 1(c) present the two compositions of the emitter. Figure 1(b) is a graphene–h-BN–graphene sandwiched structure, and Fig. 1(c) is made of two graphene–h-BN heterostructures. The thickness of the h-BN thin film is $h_{\rm BN}$ and the graphene monolayer is modeled as a layer of thickness $h_{\rm g}$. Figure 1(d) is a thin-film InSb p–n junction supported by a substrate. The thickness of the InSb thin-film is $h_{\rm InSb}$ and the substrate is set to be semi-infinite intrinsic InSb.

When the InSb cell is located at a distance d which is on the order of or smaller than the thermal wavelength $\lambda_{\rm th} = 2\pi\hbar c/k_{\rm B}T_{\rm emit}$ from the emitter, the thermal radiation can be significantly enhanced due to energy transfer via evanescent waves.[12] The radiative heat exchange between the emitter and the cell is given by[29,30]

$$Q_{\rm rad} = Q_{\omega<\omega_{\rm gap}} + Q_{\omega\geq\omega_{\rm gap}}, \tag{1}$$

where $Q_{\omega<\omega_{\rm gap}}$ and $Q_{\omega\geq\omega_{\rm gap}}$ are the heat exchanges below and above the band gap of the cell, respectively, given by

$$Q_{\omega<\omega_{\rm gap}} = \int_0^{\omega_{\rm gap}} \frac{d\omega}{4\pi^2}\big[\Theta_1(T_{\rm emit},\omega) - \Theta_2(T_{\rm cell},\omega)\big]\sum_j \int kdk\zeta_j(\omega,k), \tag{2}$$

$$Q_{\omega\geq\omega_{\rm gap}} = \int_{\omega_{\rm gap}}^{\infty} \frac{d\omega}{4\pi^2}\big[\Theta_1(T_{\rm emit},\omega) - \Theta_2(T_{\rm cell},\omega,\Delta\mu)\big]\sum_j \int kdk\zeta_j(\omega,k), \tag{3}$$

where $\Theta_1(T_{\rm emit},\omega) = \hbar\omega/[\exp(\frac{\hbar\omega}{k_{\rm B}T_{\rm emit}}) - 1]$ and $\Theta_2(T_{\rm cell},\omega,\Delta\mu) = \hbar\omega/[\exp(\frac{\hbar\omega-\Delta\mu}{k_{\rm B}T_{\rm cell}}) - 1]$ are the Planck mean oscillator energies of black body at temperatures $T_{\rm emit}$ and $T_{\rm cell}$, respectively. $\Delta\mu$ is the electrochemical potential difference across the p–n junction, which describes the effects of charge injection or depletion on the carrier recombination processes and hence modify the number of photons through the detailed balance. Here k is the magnitude of the in-plane wavevector of thermal radiation waves; $\zeta_j(\omega,k)$ is the photon transmission coefficient for the jth polarization ($j = s,p$), which consists of the contributions from both the propagating and the evanescent waves,[31]

$$\zeta_j(\omega,k) = \frac{(1-|r_{\rm emit}|^2)(1-|r_{\rm cell}|^2)}{|1-r^j_{\rm emit}r^j_{\rm cell}\exp(2ik^0_z d)|^2}, \quad k < \frac{\omega}{c},$$

$$\zeta_j(\omega,k)=\frac{4\mathrm{Im}(r^j_{\mathrm{emit}})\mathrm{Im}(r^j_{\mathrm{cell}})\exp(2ik_z^0d)}{|1-r^j_{\mathrm{emit}}r^j_{\mathrm{cell}}\exp(2ik_z^0d)|^2},\quad k\geq\frac{\omega}{c},\tag{4}$$

where $k_z^0=\sqrt{\omega^2/c^2-k^2}$ is the perpendicular-to-plane component of the wavevector in vacuum; r^j_{emit} (r^j_{cell}) with $j=s,p$ is the complex reflection coefficient at the interface between the emitter (cell) and the air. Here the reflection coefficients of the emitter and cell are calculated by the scattering matrix approach.[32,33]

Via the infrared photoelectric conversion, the above-gap radiative heat exchange is then converted into electricity. Based on the detailed balance analysis, the electric current density of an NTPV cell is given by[1,34]

$$I=I_{\mathrm{ph}}-I_0[\exp(V/V_{\mathrm{cell}})-1],\tag{5}$$

where $V=\Delta\mu/e$ is the voltage bias across the NTPV cell, $V_{\mathrm{cell}}=k_{\mathrm{B}}T_{\mathrm{cell}}/e$ is a voltage which measures the temperature of the cell.[1] I_{ph} and I_0 are the photo-generation current density and reverse saturation current density, respectively. In Eq. (5), an ideal rectifier condition has been used to simplify the nonradiative recombination.[1] The actual nonradiative mechanisms include the Shockley–Read–Hall (RSH) and Auger nonradiative processes. For the sake of simplicity, we just follow the Shockley–Queisser analysis.[1]

The reverse saturation current density is determined by the diffusion of minority carriers in the InSb p–n junction, which is given by

$$I_0=en_{\mathrm{i}}^2\Big(\frac{1}{N_{\mathrm{A}}}\sqrt{\frac{D_{\mathrm{e}}}{\tau_{\mathrm{e}}}}+\frac{1}{N_{\mathrm{D}}}\sqrt{\frac{D_{\mathrm{h}}}{\tau_{\mathrm{h}}}}\Big),\tag{6}$$

where n_{i} is the intrinsic carrier concentration, D_{e} and D_{h} are the diffusion coefficients of the electrons and holes, respectively. N_{A} and N_{D} are the p-region and n-region impurity concentrations, respectively;[35] τ_{e} and τ_{h} are correspondingly the relaxation times of the electron-hole pairs in the n-region and p-region. Numerical values of these parameters can be taken from Refs. [35,36].

The photo-generation current density is contributed from the above-gap thermal heat exchange[16,23]

$$I_{\mathrm{ph}}=\frac{e}{4\pi^2}\int_{\omega_{\mathrm{gap}}}^{\infty}\frac{d\omega}{\hbar\omega}[\Theta_1(T_{\mathrm{emit}},\omega)-\Theta_2(T_{\mathrm{cell}},\omega,\Delta\mu)]\times\sum_j\int kdk\zeta_j(\omega,k)[1-\exp[-2\mathrm{Im}(k_z^{\mathrm{InSb}})h_{\mathrm{InSb}}]],\tag{7}$$

where $k_z^{\mathrm{InSb}}=\sqrt{\varepsilon_{\mathrm{InSb}}\omega^2/c^2-k^2}$ is the perpendicular-to-plane component of the wavevector in the InSb p–n junction; $\varepsilon_{\mathrm{InSb}}$ is the dielectric function of the InSb cell, which is given by $\varepsilon_{\mathrm{InSb}}=[n+\frac{ic\alpha(\omega)}{2\omega}]^2$; $n_{\mathrm{InSb}}=4.12$ is the refractive index; c is the speed of light in vacuum; $\alpha(\omega)$ is a step-like function describing the photonic absorption, which is given by[23] $\alpha(\omega)=0$ for $\omega<\omega_{\mathrm{gap}}$ and $\alpha(\omega)=\alpha_0\sqrt{\omega/\omega_{\mathrm{gap}}-1}$ for $\omega>\omega_{\mathrm{gap}}$ with $\alpha_0=0.7\,\mu\mathrm{m}^{-1}$.[23] Since the NTPV cell is a thin film, the exponential decay characteristic of the electromagnetic wave propagating in the InSb thin-film must be considered. The term $[1-\exp[-2\mathrm{Im}(k_z^{\mathrm{InSb}})h_{\mathrm{InSb}}]]$ is the absorption probability of the incident radiation in the InSb film of thickness h_{InSb}, which measures the actual availability of the above-gap photons in the photon-carrier generation process.

The dielectric function of h-BN is described by the Drude–Lorentz model, which is given by[37]

$$\varepsilon_m=\varepsilon_{\infty,m}\Big(1+\frac{\omega_{\mathrm{LO},m}^2-\omega_{\mathrm{TO},m}^2}{\omega_{\mathrm{TO},m}^2-i\gamma_m\omega-\omega^2}\Big),\tag{8}$$

where $m=\parallel,\perp$ denotes the out-of-plane and the in-plane directions, respectively; $\varepsilon_{\infty,m}$ is the high-frequency relative permittivity, ω_{TO} and ω_{LO} are the transverse and longitudinal optical phonon frequencies, respectively; γ_m is the damping constant of the optical phonon modes. The values of these parameters are chosen as those determined by experiments.[38,39]

The effective dielectric function of the graphene monolayer is modeled as[40]

$$\varepsilon_{\mathrm{g}}=1+i\frac{\sigma_{\mathrm{g}}}{\varepsilon_0\omega h_{\mathrm{g}}},\tag{9}$$

where σ_{g} is the optical conductivity.[41]

The output electric power density P_{e} of the NTPV system is defined as the product of the net electric current density and the voltage bias,

$$P_{\mathrm{e}}=-I_{\mathrm{e}}V,\tag{10}$$

and the energy efficiency η is given by the ratio between the output electric power density P_{e} and incident radiative heat flux Q_{inc},

$$\eta=\frac{P_{\mathrm{e}}}{Q_{\mathrm{inc}}},\tag{11}$$

where the incident radiative heat flux is given by the radiative heat exchange defined in Eq. (1). The second law of thermodynamics imposes an upper bound on the energy efficiency, which is the Carnot efficiency,

$$\eta_{\mathrm{c}}=1-\frac{T_{\mathrm{cell}}}{T_{\mathrm{emit}}}.\tag{12}$$

When studying the energy efficiency of various NTPV systems with different temperatures, we use the Carnot efficiency to quantify and compare their energy efficiencies.

Performances of Graphene–h-BN-InSb Near-Field Systems. We first examine the performances of the two types of NTPV cells. Figure 2 shows the output power density and energy efficiency as a function of voltage bias for the two setups, respectively, denoted as the G-FBN-G-InSb cell (graphene–h-BN–graphene

heterostructure as the emitter and thin-film InSb p–n junction as the receiver) and the G-FBN-G-FBN-InSb cell (graphene–h-BN–graphene–h-BN heterostructure as the emitter and thin-film InSb p–n junction as the receiver). The output power density and energy efficiency are optimized for various physical parameters, including the temperature of the cell, the chemical potential of graphene and h-BN film thickness.[28] The analysis in Ref. [28] shows that setting $\mu_g = 1.0\,\text{eV}$, $h_{BN} = 20\,\text{nm}$ and $T_{cell} = 320\,\text{K}$ provides roughly optimal performance, both in terms of power and efficiency, for the NTPV systems considered in this work. Therefore, these parameters are kept as those constants in the main text. The thickness of the InSb thin film is set as $h_{InSb} = 1000\,\text{nm}$, which is close to the thickness of experimental samples.[42]

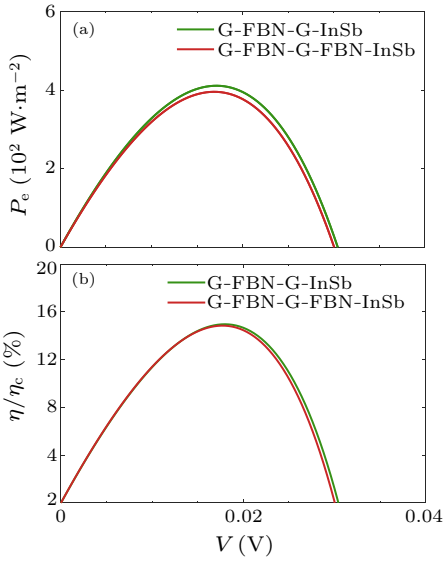

Fig. 2. Performances of two NTPV cells. (a) Electrical power density and (b) energy-conversion efficiency in units of Carnot efficiency (η_c). The temperatures of the emitter and the cell are set at $T_{emit} = 450\,\text{K}$ and $T_{cell} = 320\,\text{K}$, respectively. The vacuum gap distance is $d = 20\,\text{nm}$, the h-BN film thickness is $h_{BN} = 20\,\text{nm}$ and the thickness of the InSb thin film is $h_{InSb} = 1000\,\text{nm}$. The chemical potential of graphene is $\mu_g = 1.0\,\text{eV}$. The Carnot efficiency is given by $\eta_c = 1 - T_{cell}/T_{emit}$.

As shown in Fig. 2, the maximum output power density of the G-FBN-G-InSb cell is about $4.1 \times 10^2\,\text{W/m}^2$, nearly 1.1 times of the maximum output power density of the G-FBN-G-FBN-InSb cell (about $3.9 \times 10^2\,\text{W/m}^2$). For the energy-conversion efficiency, the maximum values of the G-FBN-G-InSb cell is about $0.15\eta_c$, which is slightly higher than the maximum efficiency of the FBN-G-FBN-InSb cell (about $0.149\eta_c$).

In order to analyze the physical mechanisms responsible for such performances of these two setups, we show the spectral distributions of the photo-induced current and incident radiative heat flux at the maximum electric power density for the G-FBN-G-InSb and G-FBN-G-FBN-InSb cells in Fig. 3. The two shaded areas in Figs. 3(a) and 3(b) are the two reststrahlen bands of h-BN.[43] As exhibited in Fig. 3(a), higher photo-induced current spectra of the two systems appear at and near the reststrahlen band due to the reststrahlen effect. The reststrahlen effect originates from the hyperbolic optical properties of the h-BN film due to the photon–optical-phonon interactions. In the reststrahlen band presented in Fig. 3(a), the in-plane dielectric function of h-BN is negative, leading to strong reflection and suppressed transmission of incident photons.[43] The near-field radiation effects are essentially caused by the evanescent propagation of the incident photons, which dramatically enhances the radiative heat transfer between two closed spaced objects.[24–28,37,44] Such enhancement of the radiative heat transfer eventually leads to the significant increase of the input heat flux, output electric power and the energy efficiency.[28]

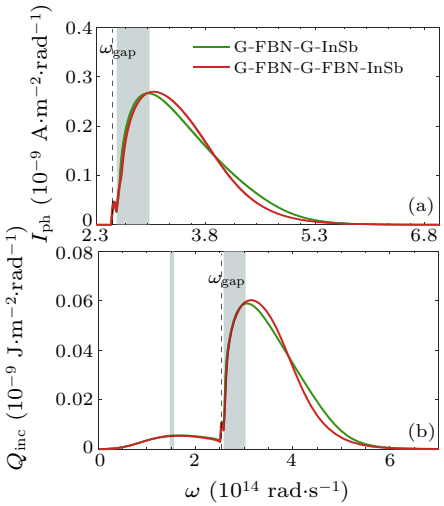

Fig. 3. (a) Photo-induced current spectra $I_{ph}(\omega)$ and (b) incident radiative heat spectra $Q_{inc}(\omega)$ at the maximum electric power density for the two configurations. The temperatures of the emitter and the cell are kept at $T_{emit} = 450\,\text{K}$ and $T_{cell} = 320\,\text{K}$, respectively. The vacuum gap is $d = 20\,\text{nm}$ and the chemical potential of graphene is set as $\mu_g = 1.0\,\text{eV}$. The h-BN film thickness is $h_{film} = 20\,\text{nm}$. The chemical potential difference across the InSb p–n junction $\Delta\mu$ is optimized independently for maximum output power for each configuration.

It is noticed that the overall photo-induced current spectrum of the G-FBN-G-InSb cell is higher than the one of the G-FBN-G-FBN-InSb cell except in the frequency range from $3.1 \times 10^{14}\,\text{rad/s}$ to $4.1 \times 10^{14}\,\text{rad/s}$. After integrating over ω, this higher photo-induced current spectrum gives rise to improved output power of the G-FBN-G-InSb cell.

Contrarily to the photo-induced current spectra, the overall incident radiative heat flux of the G-FBN-G-FBN-InSb cell is higher than the G-FBN-G-InSb cell. Since the energy-conversion efficiency is defined as the ratio of the output electric power density and

the incident radiation heat flux, the higher output power density and the lower incident radiation heat flux give a higher energy efficiency of the G-FBN-G-InSb cell.

To further elucidate the mechanism for the enhanced performance of the near-field systems, we examine the photon tunneling coefficient $\zeta_j(\omega, k)$ [given by Eq. (4)]. As shown in Fig. 4, the bright color indicates a high transmission coefficient. The green dashed lines are the light lines of vacuum and InSb, respectively. Note that the maximum transmission coefficient is 2 due to the contribution of both s and p polarizations. In the above-gap range, both G-FBN-G-InSb cell and G-FBN-G-FBN-InSb cell exhibit enhanced photon transmission, thanks to the SPPPs supported by the graphene–h-BN heterostructures. Figure 4 shows that the photon transmission spectra of the two near-field NTPV systems do not differ much. Therefore, the performances of the two NTPV systems are comparable.

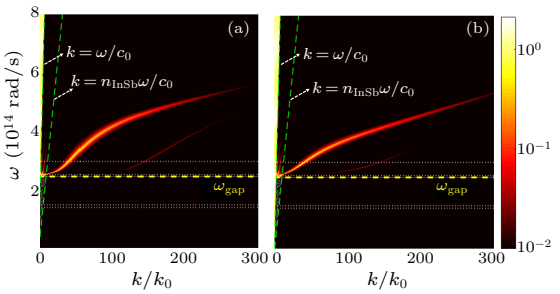

Fig. 4. Photon transmission coefficient $\zeta(\omega, k)$ for (a) G-FBN-G-InSb cell and (b) G-FBN-G-FBN-InSb cell. The temperatures of the emitter and the cell are kept at $T_{\rm emit} = 450\,{\rm K}$ and $T_{\rm cell} = 320\,{\rm K}$, respectively. The vacuum gap is $d = 20\,{\rm nm}$ and the chemical potential of graphene is set as $\mu_{\rm g} = 1.0\,{\rm eV}$. The h-BN film thickness is $h_{\rm film} = 20\,{\rm nm}$ and the InSb thin-film thickness is $h_{\rm InSb} = 1000\,{\rm nm}$.

Optimization of Graphene–h-BN–InSb Near-Field Systems. We now study the performances of the two near-field systems for various InSb thin-film thicknesses and emitter temperatures in Figs. 5 and 6. As presented in Fig. 5 that both of the output power density and the energy-conversion efficiency of the two setups are improved with increasing the InSb thin-film thickness. Especially for $h_{\rm InSb} = 10000\,{\rm nm}$, the maximum power densities of the G-FBN-G-InSb cell and G-FBN-G-FBN-InSb cell are about $4.5 \times 10^2\,{\rm W/m^2}$ and $4.0 \times 10^2\,{\rm W/m^2}$, respectively. The maximum values of the corresponding efficiency are close to $0.16\eta_{\rm C}$ and $0.15\eta_{\rm C}$, respectively. This enhancement can be attributed to the increased absorption factor $[1 - \exp[-{\rm Im}(k_z^{\rm InSb})h_{\rm InSb}]]$ because it is dependent on $h_{\rm InSb}$. However, when the InSb thin-film thickness is increased from 4000 nm to 10000 nm, the increase of the output power density and the energy-conversion efficiency for both systems are soon saturated. This is essentially due to the near-field nature of the heat transfer: the photons transferred from the emitter to the InSb cell is dominated by the evanescent electromagnetic waves which are highly localized at the surface of the emitter. Further increase of the thickness of the InSb cell does not change the amount of photons received by the InSb cell.

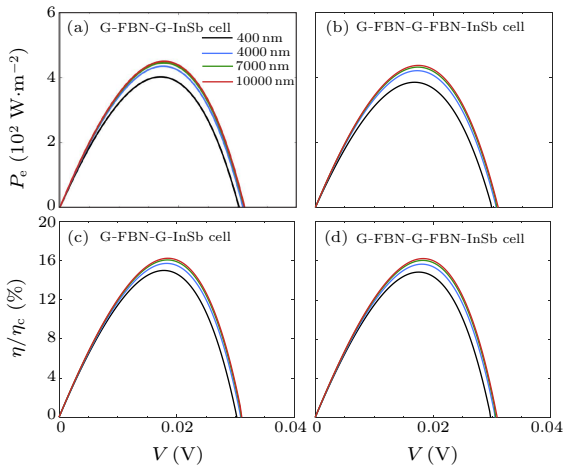

Fig. 5. Performances of two near-field TPV cells for various InSb thin-film thickness. (a) Electrical power density and (b) energy-conversion efficiency in units of Carnot efficiency ($\eta_{\rm c}$). The temperatures of the emitter and the cell are set at $T_{\rm emit} = 450\,{\rm K}$ and $T_{\rm cell} = 320\,{\rm K}$, respectively. The vacuum gap distance is $d = 20\,{\rm nm}$, the h-BN film thickness is $h_{\rm BN} = 20\,{\rm nm}$ and the chemical potential of graphene is $\mu_{\rm g} = 1.0\,{\rm eV}$.

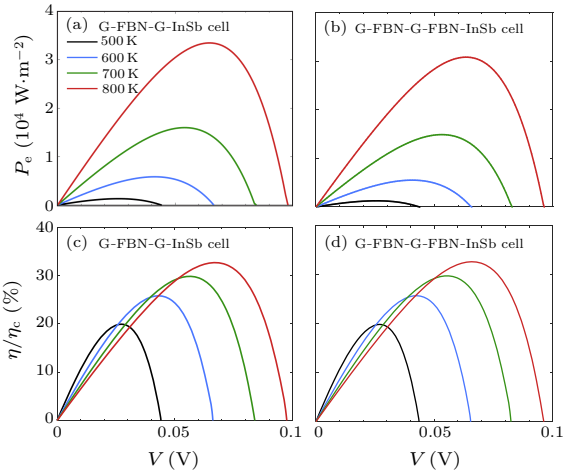

Fig. 6. Performances of two near-field TPV cells for various emitter temperatures. (a) Electrical power density and (b) energy-conversion efficiency in units of Carnot efficiency ($\eta_{\rm c}$). The temperature of the cell is set at $T_{\rm cell} = 320\,{\rm K}$. The vacuum gap distance is $d = 20\,{\rm nm}$, the h-BN film thickness is $h_{\rm BN} = 20\,{\rm nm}$ and the thickness of the InSb thin film is chosen as an optimal value of $h_{\rm InSb} = 10000\,{\rm nm}$. The chemical potential of graphene is $\mu_{\rm g} = 1.0\,{\rm eV}$.

Figure 6 shows that by increasing the emitter temperature, both the performances of the two setups can be improved by orders of magnitudes. Here, the InSb thin-film thickness has been chosen as the opti-

mal value with $h_{\mathrm{InSb}} = 10000\,\mathrm{nm}$. For the G-FBN-G-InSb cell, the maximum output power density and energy efficiency at $T_{\mathrm{emit}} = 800\,\mathrm{K}$ are increased to $3.3 \times 10^4\,\mathrm{W/m^2}$ and $0.33\eta_{\mathrm{c}}$, respectively. For the G-FBN-G-FBN-InSb cell, the maximum output power density and energy efficiency at $T_{\mathrm{emit}} = 800\,\mathrm{K}$ are also improved to $3.1 \times 10^4\,\mathrm{W/m^2}$ and $0.32\eta_{\mathrm{c}}$, respectively.

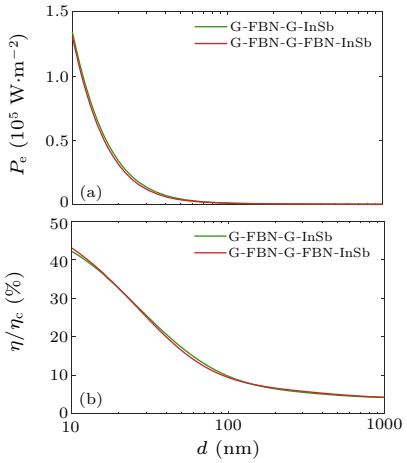

Fig. 7. Optimal performances of two NTPV cells. (a) Maximum electrical power density and (b) energy-conversion efficiency at maximum electric power in units of Carnot efficiency (η_{c}). The temperatures of the emitter and the cell are set at $T_{\mathrm{emit}} = 800\,\mathrm{K}$ and $T_{\mathrm{cell}} = 320\,\mathrm{K}$, respectively. The h-BN film thickness is $h_{\mathrm{BN}} = 20\,\mathrm{nm}$ and the thickness of the InSb thin film is $h_{\mathrm{InSb}} = 10000\,\mathrm{nm}$. The chemical potential of graphene is $\mu_{\mathrm{g}} = 1.0\,\mathrm{eV}$. The Carnot efficiency is given by $\eta_{\mathrm{c}} = 1 - T_{\mathrm{cell}}/T_{\mathrm{emit}}$.

We now examine the maximum output electric power density and the efficiency at maximum power. We consider specifically the situation with $h_{\mathrm{InSb}} = 10000\,\mathrm{nm}$ and $T_{\mathrm{emit}} = 800\,\mathrm{K}$. As shown in Fig. 7, both the maximum electric power density and the efficiency at the maximum power of the two near-field NTPV systems dramatically increase as the vacuum gap d decreases. The best performances are achieved when the vacuum gap is $d = 10\,\mathrm{nm}$ for both the systems. Specifically, the maximum electric power density reaches $1.3 \times 10^5\,\mathrm{W/m^2}$, while the efficiency at maximum power goes up to 42% of the Carnot efficiency. The two near-field NTPV systems perform nearly equally well.

In summary, we have investigated two NTPV devices, denoted as the G-FBN-G-InSb cell and the G-FBN-G-FBN-InSb cell, which have different emitters. The purpose of the investigation is to find a high-performance emitter design with relatively simple structure. Indeed, we find that both the systems perform better than the near-field NTPV system based on mono graphene–h-BN heterostructure, i.e., graphene–h-BN–InSb cell.[28] The optimal output power density of the G-FBN-G-InSb cell can reach to $1.3 \times 10^5\,\mathrm{W/m^2}$, nearly twice of the optimal power density of the graphene–h-BN–InSb cell. The optimal energy efficiency can be as large as 42% of the Carnot efficiency, which is 24% higher than the optimal efficiency of the monocell system. We analyze the underlying physical mechanisms that lead to the excellent performances of the G-FBN-G-InSb cell. It is further shown that the performance of the proposed NTPV system is affected negligibly by the finite thickness of the InSb cell, which is due to the near-field nature of the heat transfer: the absorbed photons are highly localized at the surface of the InSb cell. Our study shows that NTPV systems are promising for high-performance moderate temperature thermal-to-electric energy conversion.

References

[1] Shockley W and Queisser H J 1961 *J. Appl. Phys.* **32** 510
[2] Martín D and Algora C 2004 *Semicond. Sci. Technol.* **19** 1040
[3] Nagashima T, Okumura K and Yamaguchi M 2007 *AIP Conf. Proc.* **890** 174
[4] Fraas L M and Ferguson L G 2000 *US Patent 6091018*
[5] Sulima O V and Bett A W 2001 *Sol. Energy Mater. Sol. Cells* **66** 533
[6] Wu C, Neuner I B, John J, Milder A, Zollars B, Savoy S and Shvets G 2012 *J. Opt.* **14** 024005
[7] Chan W R, Bermel P, Pilawa-Podgurski R C N, Marton C H, Jensen K F, Senkevich J J, Joannopoulos J D, Soljačić M and Celanovic I 2013 *Proc. Natl. Acad. Sci. USA* **110** 5309
[8] Liao T, Cai L, Zhao Y and Chen J 2016 *J. Power Sources* **306** 666
[9] Zhao B, Chen K, Buddhiraju S, Bhatt G, Lipson M and Fan S 2017 *Nano Energy* **41** 344
[10] Tervo E, Bagherisereshki E and Zhang Z M 2018 *Front. Energy* **12** 5
[11] Svetovoy V B, Van Zwol P J and Chevrier J 2012 *Phys. Rev. B* **85** 155418
[12] Ilic O, Jablan M, Joannopoulos J D, Celanovic I and Soljačić M 2012 *Opt. Express* **20** A366
[13] Svetovoy V B and Palasantzas G 2014 *Phys. Rev. Appl.* **2** 034006
[14] Basu S, Yang Y and Wang L 2015 *Appl. Phys. Lett.* **106** 033106
[15] Narayanaswamy A and Chen G 2003 *Appl. Phys. Lett.* **82** 3544
[16] Laroche M, Carminati R and Greffet J J 2006 *J. Appl. Phys.* **100** 063704
[17] Park K, Basu S, King W P and Zhang Z M 2008 *J. Quant. Spectrosc. Radiat. Transfer* **109** 305
[18] Bright T J, Wang L P and Zhang Z M 2014 *J. Heat Transfer* **136** 062701
[19] Molesky S and Jacob Z 2015 *Phys. Rev. B* **91** 205435
[20] St-Gelais R, Bhatt G R, Zhu L, Fan S and Lipson M 2017 *ACS Nano* **11** 3001
[21] Jiang J H and Imry Y 2018 *Phys. Rev. B* **97** 125422
[22] Papadakis G T, Buddhiraju S, Zhao Z, Zhao B and Fan S 2020 *Nano Lett.* **20** 1654
[23] Messina R and Ben-Abdallah P 2013 *Sci. Rep.* **3** 1383
[24] Woessner A, Lundeberg M B, Gao Y, Principi A, Alonso-González P, Carrega M, Watanabe K, Taniguchi T, Vignale G, Polini M, H J, Hillenbrand R and Koppens F H L 2015 *Nat. Mater.* **14** 421
[25] Zhao B and Zhang Z M 2017 *J. Heat Transfer* **139** 022701
[26] Zhao B, Guizal B, Zhang Z M, Fan S and Antezza M 2017 *Phys. Rev. B* **95** 245437
[27] Shi K, Bao F and He S 2017 *ACS Photon.* **4** 971

[28] Wang R, Lu J and Jiang J H 2019 *Phys. Rev. Appl.* **12** 044038
[29] Polder D and Van H M 1971 *Phys. Rev. B* **4** 3303
[30] Pendry J B 1999 *J. Phys.: Condens. Matter* **11** 6621
[31] Mulet J P, Joulain K, Carminati R and Greffet J J 2002 *Nanoscale Microscale Thermophys. Eng.* **6** 209
[32] Whittaker D M and Culshaw I S 1999 *Phys. Rev. B* **60** 2610
[33] Zhang Z M 2007 *Nano/Microscale Heat Transfer* (New York: McGraw-Hill)
[34] Ashcroft N W and Mermin N D 1976 *Solid State Physics* (Philadelphia: Scientific Research)
[35] Shur M S 1996 *Handbook Series On Semiconductor Parameters* (Singapore: World Scientific) vol 1
[36] Lim M, Jin S, Lee S S and Lee B J 2015 *Opt. Express* **23** A240
[37] Kumar A, Low T, Fung K H, Avouris P and Fang N X 2015 *Nano Lett.* **15** 3172
[38] Geick R, Perry C H and Rupprecht G 1966 *Phys. Rev.* **146** 543
[39] Caldwell J D, Kretinin A V, Chen Y, Giannini V, Fogler M M, Francescato Y, Ellis C T, Tischler J G, Woods C R, Giles A J, Hong M, Watanabe K, Taniguchi T, Maier S A and Novoselov K S 2014 *Nat. Commun.* **5** 5221
[40] Vakil A and Engheta N 2011 *Science* **332** 1291
[41] Falkovsky L A 2008 *J. Phys.: Conf. Ser.* **129** 012004
[42] Yang T R, Cheng Y, Wang J B and Feng Z C 2006 *Thin Solid Films* **498** 158
[43] Jacob Z 2014 *Nat. Mater.* **13** 1081
[44] Brar V W, Jang M S, Sherrott M, Kim S, Lopez J J, Kim L B, Choi M and Atwater H 2014 *Nano Lett.* **14** 3876